SAND2000-1548C

A miniature, high-resolution laser radar operating at video rates

Colin L. Smithpeter, Robert O. Nellums, Steve M. Lebien, George Studor*

Sandia National Laboratories, P.O. Box 5800, Albuquerque, N.M. 87185-0860
Sandia is a multiprogram laboratory operated by Sandia Corporation, a Lockheed Martin Company, for the United States Department of Energy under contract DE-AC04-94AL85000.

*NASA Johnson Space Center, Mail Code ES1, 2101 NASA Rd 1, Houston,TX 77058

ABSTRACT

We are developing a laser radar to meet the needs of NASA for a 5-lb, 150 in^3 image sensor with a pixel range accuracy of 0.1-inch. NASA applications include structural dynamics measurements, navigation guidance in rendezvous and proximity operations, and space vehicle inspection. The sensor is based on the scannerless range imager architecture developed at Sandia. This architecture modulates laser floodlight illumination and a focal plane receiver to phase encode the laser time of flight (TOF) for each pixel. We believe this approach has significant advantages over architectures directly measuring TOF including high data rate, reduced detector bandwidth, and conventional FPA detection. A limitation of the phase detection technique is its periodic nature, which provides relative range information over a finite ambiguity interval. To extend the operating interval while maintaining a given range resolution, a LADAR sensor using dual modulation frequencies has been developed. This sensor also extends the relative range information to absolute range by calibrating a gating function on the receiver to the TOF. The modulation frequency values can be scaled to meet the resolution and range interval requirements of different applications. Results from the miniature NASA sensor illustrate the advantages of the dual-frequency operation and the ability to provide the range images of 640 by 480 pixels at 30 frames per second.

Keywords: Range, imaging, laser, time of flight, heterodyne, phase, modulation, miniature, fine resolution

1. INTRODUCTION

This paper describes the development of a compact laser radar (LADAR) for object characterization and guidance in the exploration of space. The immediate application for the 3-D imagery is on-orbit mechanical dynamics measurements of the International Space Station (ISS). Other space application include vehicle inspection (e.g. shuttle heat shield) and guidance for proximity operations such as rendezvous, docking, and station keeping.

NASA has conducted extensive numerical analysis of the ISS to verify its structural integrity and estimate its lifetime. This analysis is sensitive to lightly damped modes, which are verified by on-orbit measurements. Experiments are planned to quantify the modes by measuring the vibration induced in the ISS by shuttle thruster excitation. Current instrumentation consisting of accelerometers and photogrametery provides limited sampling of the induced vibration. An innovative solution to the sampling problem is to image the vibration as a function of time and spatial location using a LADAR sensor. The LADAR requirements for the vibration mode imaging are demanding. To minimize the magnitude of the excitation and the number of excitation events, the subsequent stress on the ISS, dynamic range resolution of 0.1 inches is required over a 40 degree field of view. The sensor must provide absolute range to 150 feet with 1 inch stability to provide coverage of the entire ISS from one

vantage point and cohesion between the data in separate fields of view (FOV). Because the LADAR could operate with astronauts in the FOV, the laser illumination must be eye-safe. Finally, because no modifications to the standard camera are feasible for the experiment, the sensor must weigh less than 5 pounds and fit into a 10x6x3-inch volume.

This paper describes the development of a LADAR sensor for the structural dynamics application. The sensor measures the laser time of flight (TOF) to the scene and back by heterodyning the intensity modulated illumination with a receiver gain modulation. This LADAR technique has been previously described [1-4] as a Scannerless Range Imager (SRI). Under NASA development, the sensor is named the Laser Dynamic Range Imager (LDRI). The innovations developed in the LDRI include its compact size, small weight, sub-inch range resolution, absolute range over 150 feet, MHz range pixel rate, and eye safe laser illumination.

2. SENSOR DESCRIPTION

Figure 1 is a photo of the engineering development sensor delivered to NASA Johnson Space Center (JSC) for pre-flight testing. The sensor met size and weight requirements at 5 pounds and 2.3x5.9x11.5 inches. A space qualified flight unit currently being assembled is 3.0x4.6x10.0 inches and weighs 4 pounds, 3 ounces. Within the sensor is an 805 nm laser diode illuminator providing up to 12 W of power. The laser emits intensity modulated, continuous wave (CW) bursts of illumination at either 3.125 MHz or 140 MHz. The significance of the two frequencies is explained in a following section. The laser light is expanded to a 2 inch diameter and passed through a diffuser plate, visible on the right side of the photo, to floodlight illuminate the scene. Diffuser plates with half-power angles varying from 10 to 60 degrees are available. The maximum eye safety risk occurs at the diffuser where the laser power density is greatest. For the ANSI worst case exposure of 10 s, the maximum permissible exposure is 0.31 W/cm^2 with the extended source correction term. The measured power density at the closest eye assessable distance of 2 cm is 0.23 W/cm2 with the nominal 40 degree diffuser, which is an eye-safe power density. The diffuser diameter in the flight unit is three inches to improve this safety margin.

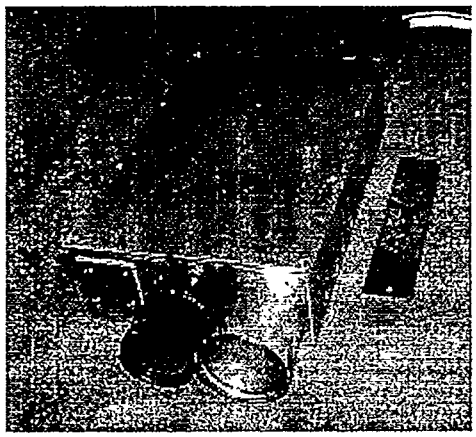

Figure 1: Photograph of engineering development LADAR sensor. A six-inch ruler is included to indicate scale.

A conventional camera lens images the reflected laser light from the scene onto the cathode of an image intensifier tube. A 30 nm bandpass filter on the lens limits background light contribution. The

DISCLAIMER

intensifier optical gain is sinusoidally modulated by varying the micro-channel plate voltage within the tube at the laser modulation frequency. A gating function is applied to the cathode potential to eliminate return from outside the desired range interval as well as limiting the ambient light contribution. A fiber optic taper couples the intensified image on the phosphor output screen to a CCD detector. The CCD is read out by a conventional analog video camera at 30 frames per second.

No additional cables could be added to the shuttle for our application so the sensor is interfaced to the shuttle video system for data input and output. Image data is retrieved from the sensor as standard RS-170 video at 30 frames per second. Commands to the sensor are encoded within the video synchronization intervals. For real-time processing and visualization, the data is received and processed by a laptop computer in the shuttle flight deck. The video is also recorded onto tape for detailed post-flight analysis.

Range TOF algorithm

The SRI technique is to illuminate the scene with a modulated, diffuse source, and to measure the average reflected intensity with an imaging receiver incurring modulated gain. A sequence of intensity images is obtained at discrete steps in the relative modulation phase between the receiver and source. The range-processing algorithm deduces range based on the observed relationship between intensity and phase or frequency of modulation. Relative to other LADAR techniques, the SRI advantages include a solid-state architecture, reduced detector bandwidth, fewer data dropouts, and the use of conventional focal plane array (FPA) technology. The following paragraphs provide a detailed description of the technique.

Since the transmitter and receiver modulation waveforms are periodic, they may be represented as a Fourier series:

$$XMT(t) = A_0 + \sum_{i=1}^{\infty} A_i Cos\left(i2\pi f_0 t + \alpha_i\right) \tag{1}$$

$$RCV(t) = B_0 + \sum_{j=1}^{\infty} B_j Cos\left(j2\pi f_0 t + \beta_j + j\theta_n\right) \tag{2}$$

The fundamental modulation frequency is defined as $\mathbf{f_0}$, and relative phase between the transmitter and receiver waveform is varied discretely, from image-frame to image-frame by the θ_n term. The convention is to use the indices, **i** and **j**, to refer to harmonic order of the modulation-waveform component, while "n" refers to the image number. The α_i and β_j terms are fixed components of transmitter and receiver timing at each harmonic. The $\theta_n/(2\pi f_0)$ term is the additional time delay between transmitter and receiver modulation during the nth image.

The illumination at range R, and time t, was transmitted at **(t-R/c)** and is imaged at time **(t+R/c)**. The instantaneous pixel brightness of the nth image after receiver demoduation may be represented as:

$$I_n\left(t+\frac{R}{c}\right) = \left[A_0 + \sum_{i=1}^{\infty} A_i Cos\left(i2\pi f_0\left(t-\frac{R}{c}\right)+\alpha_i\right)\right] * \left[B_0 + \sum_{j=1}^{\infty} B_j Cos\left(j2\pi f_0\left(t+\frac{R}{c}\right)+\beta_j + j\theta_n\right)\right] \tag{3}$$

The **A** and **B** coefficients in the above equation include both sensor dependent and scene dependent parameters, such as background and reflectance.

Terms in the above equation may be restated as:

$$I_n\left(t+\frac{R}{c}\right)=A_0B_0+\frac{1}{2}\sum_{i=1}^{\infty}\sum_{j=1}^{\infty}A_iB_j\left[\begin{array}{l}Cos\left(2\pi f_0\left((j-i)t+(j+i)\frac{R}{c}\right)+\beta_j-\alpha_i+j\theta_n\right)\\+Cos\left(2\pi f_0\left((j+i)t+(j-i)\frac{R}{c}\right)+\beta_j+\alpha_i+j\theta_n\right)\end{array}\right] \quad (4)$$

The time constant of the intensifier phosphor screen and the camera integration period are assumed to have a duration of many thousands of modulation periods at frequency f_0, which provides a means for detecting the DC component of this signal. Since all time dependant terms at frequency f_0, or above, will null during integration, the remaining significant terms are:

$$I_n=A_0B_0+\frac{1}{2}\sum_{i=1}^{\infty}A_iB_iCos\left(\frac{4\pi f_0iR}{c}+\beta_i-\alpha_i+i\theta_n\right) \quad (5)$$

The subscript, i, denotes the order of the harmonic, relative to the fundamental modulation frequency. In order for a harmonic to be present, it is necessary that it be present in both transmitted and received waveforms, so that both A_i and B_i are non-zero.

If either the laser or gain modulation contains only the fundamental frequency, the equation for measured intensity, I, contains three unknowns, A_0B_0, A_1B_1, and the relative range. Assume that R is a constant and that a total of N images are collected, with equal phase increments, such that $\theta_n=2\pi n/N$. Then the discrete Fourier transform may be applied to I_n, for i=1 to (N-1)/2:

$$\left\{\frac{A_iB_i}{2}Cos\left(\frac{4\pi f_0iR}{c}+\beta_i-\alpha_i\right)\right\}\cong\frac{2}{N}\sum_{n=1}^{N}I_nCos\left(\frac{2\pi ni}{N}\right) \quad (6)$$

$$\left\{\frac{A_iB_i}{2}Sin\left(\frac{4\pi f_0iR}{c}+\beta_i-\alpha_i\right)\right\}\cong-\frac{2}{N}\sum_{n=1}^{N}I_nSin\left(\frac{2\pi ni}{N}\right)$$

From this, one may state:

$$\left\{\frac{4\pi f_0R}{c}+\beta_1-\alpha_1\right\}\cong ATAN\left(\frac{\sum_{n=1}^{N}I_nCos\left(\frac{2\pi n}{N}\right)}{-\sum_{n=1}^{N}I_nSin\left(\frac{2\pi n}{N}\right)}\right) \quad (7)$$

The result is an efficient algorithm, having a full 2π interval for relative range, which is not reliant upon an initial estimate for A_1B_1/A_0B_0. The term on the left side of the equation is called relative range. The $(\beta-\alpha)$ term is a fixed timing delay associated with the electronics that is measured and calibrated to absolute range within each ambiguity interval.

The NASA sensor uses a four image sample architecture (N=4), which simplifies the range calculation to:

$$\frac{4\pi f_0R}{c}+\beta_1-\alpha_1=ATAN\left(-I_2+I_4\,/\,-I_1+I_3\right) \quad (8)$$

This 4-point algorithm is particularly efficient, being two differences and an ARCTAN function. The algorithm may be faster if the trigonometric function is replaced by a look-up table. In addition, the electronics associated with 90° phase increments are easiest to implement.

Sensor Design

A primary design challenge in the NASA sensor is the required range accuracy. The following section derives the balance between modulation frequency and signal to noise ratio needed for the 0.1 inch range accuracy. Neglecting harmonics, the signal energy contained in N samples would be $N(A_1B_1/2)^2/2$. For all values of N, the phase calculation partitions an energy of $2\sigma^2$ into the A_1B_1 /2 term, of which σ^2 is in phase with signal energy and σ^2 is out of phase with signal energy. The error in computing the phase of "relative range" is approximated by the square root of quadrature noise energy divided by signal energy. On this basis, rms noise in the calculated range is expressed as:

$$Range\,Noise_{rms} = \frac{c}{2\pi f_0}\frac{\sigma}{\left(A_1B_1/2\right)}\sqrt{\frac{2}{N}} \tag{9}$$

The fundamental coefficients A_1B_1 can be approximated to the depth of intensity modulation observed across the image samples. Based on RF component availability, we selected 140 MHz for the modulation frequency. If the worst-case camera noise is 2 A/D counts, the required modulation is 95 counts for 0.1 inch accuracy, which was a viable requirement.

A limitation of heterodyne TOF detection is the periodic nature of the range data. If the spread in laser TOF returns span more than one receiver oscillation, objects separated by the ambiguity interval can have the same measured phase and range. The ambiguity interval is equal to:

$$R_{amb} = c/2f_0 \tag{10}$$

where c is the speed of light. To meet the requirement for absolute range over 150 ft, a second modulation frequency of 3.125 MHz is used in a alternate acquisition to the 140 MHz modulation. The range data from the 3 MHz image is used as a coarse resolution to determine the integer number of ambiguity intervals for each pixel at 140 MHz. With the two frequency operation, the sensor provides absolute range with 0.1 accuracy over a 158 foot interval.

3. RESULTS

At 140 MHz modulation, the measured range accuracy in each pixel is 0.22 inch at 30 frames/second acquisition. The measured accuracy compares well with the estimated 0.16 inch accuracy from Equation 9 using the measured 1.35 count standard deviation and 80 count depth of modulation. To reach the desired accuracy of 0.1 inches at video rate acquisition, six pixels must be averaged within or across the video images. Averaging is acceptable since the sensor is looking at surfaces spanning many pixels and provides 640 by 480 pixels in each image. If 100 frames are averaged to improve the signal to noise ratio, we have observed range accuracy of 0.01 inches in laboratory conditions.

We conducted several experiments to validate the vibration measurements of the system. Figure 2 is a plot of the displacement as a function of time and the calculated vibration spectra from a vibrating flat plate. The vibration spectrum indicates a fundamental frequency at 0.6 Hz.

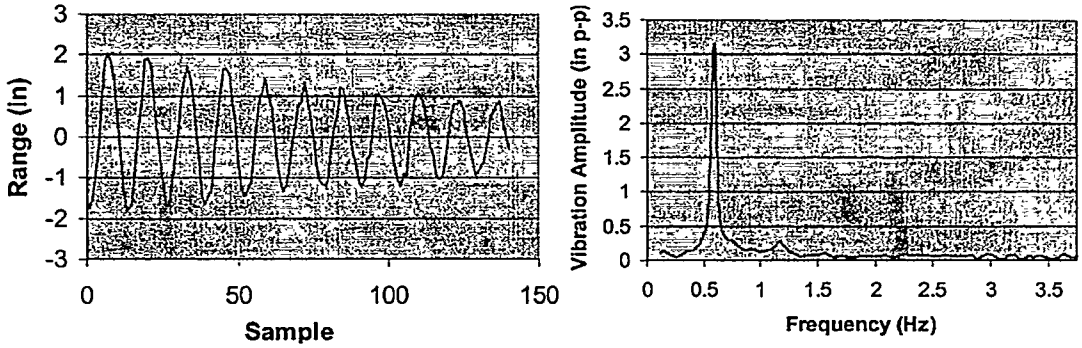

Figure 2: Measured displacement as function of image number at 30 fps (left) and the calculated frequency spectrum.

In another laboratory experiment, we imaged a model of the ISS solar array while deflecting the tip of the array. Figure 3 shows a 140 MHz image of the array and the measured displacement versus time. Other information available from the range imagery includes absolute range, range rate, and angular orientation relative to the sensor.

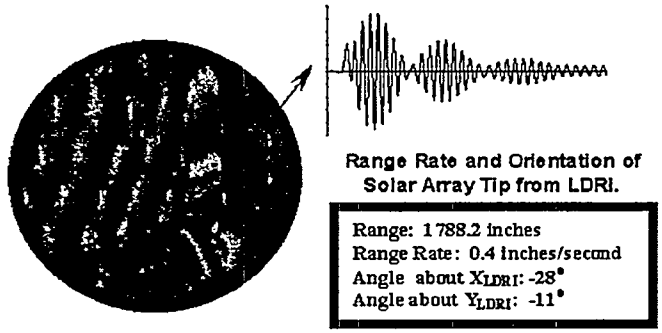

Figure 3: A 140 MHz image from the solar array model, plot of displacement vs. time from the area of the box, and the information available from the LDRI data.

To demonstrate the absolute range stability and 0.1 inch range accuracy, we conducted an experiment to detect small changes in the imaged scene. Figure 4 displays the laser reflectance and range image taken of a perimeter fence from a 40 foot tower. After capturing a baseline range image, a person and vehicle traversed the scene in front of the fence. A second range image was acquired and subtracted from the baseline image.

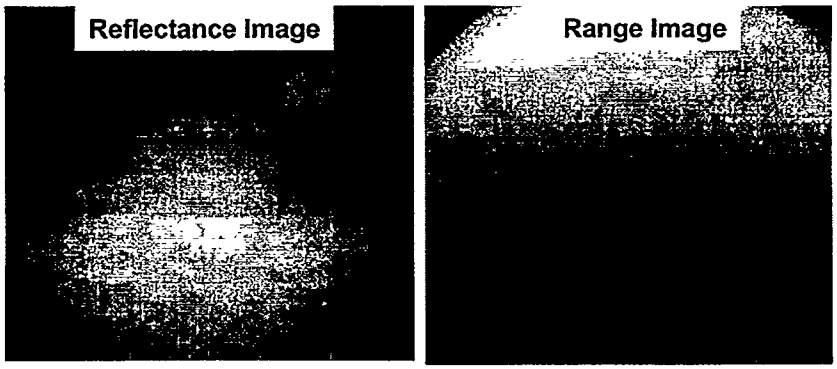

Figure 4: Laser reflectance and range image of perimeter fence taken from a 40 foot tower.

The difference image in Figure 5 indicates the LDRI range accuracy and stability are sufficient to resolve the footprints and tire tracks. The time between the baseline and the second image was approximate 20 minutes. The grayscale of the difference range image has been scaled to cover a 0.7 inch distance. The appearance of fence posts at the top of the difference image is caused by tower motion. A 3-D surface rendering of the footprint in Figure 5 illustrates the available detail in the heel and toe of the impression. A third range image with the field of view reduced to 20 degrees resolved the individual treads in the tire track, as shown in the surface rendering in Figure 5.

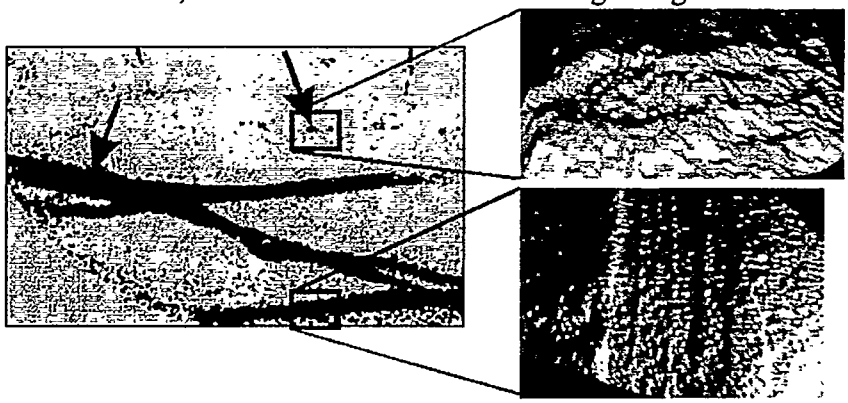

Figure 5: Range difference image (left) showing the footprints and tire tracks created between the baseline and second acquisition. Surface renderings (right) of the range image show the details of the impressions.

In addition to the vibration spectra, the range pixel rate of 2.3×10^6 allows for 3-D capture of motion sequences. Figure 6 contains a series of images selected from a 60 second range video of the sensor being rolled down an office hallway at 2 feet per second. In these raw range images, increasing brightness indicates increasing range. The range images exhibit motion induced artifacts at edges of large discontinuity in range, such as a corner or doorway. The arrows in Figure 6 point to the artifacts that appear as shifts in the grayscale value, often to black or white. If the range to a pixel changes during the four image acquisition needed to calculate range, the constant range assumption of Equation 6 is violated and erroneous range is calculated.

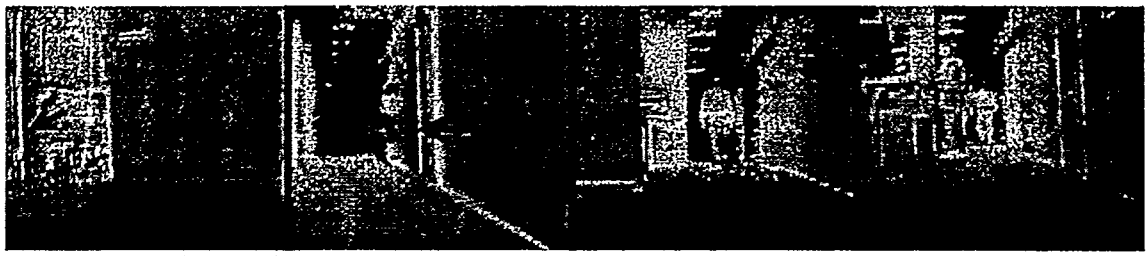

Figure 6: Selected range images from a 60 second sequence recorded by the LDRI on a cart moving down a hallway at 2 feet per second. Arrows indicate areas of motion artifact.

4. SUMMARY

We have developed an advanced LADAR sensor for space exploration applications including structure characterization and proximity navigation. The immediate application of structural dynamics

measurements has demanding requirements of 0.1 inch accuracy over a 40 degree field of view with 30 Hz acquisition rates. The SRI phase detection technique is uniquely suited for the structural application because of increased range accuracy for a given detector bandwidth and the use of conventional focal plane array detectors with MHz pixel rates. Other advancements include its small size and weight, absolute range over 150 foot intervals, and eye safe illuminator.

5. REFERENCES

1. M. W. Scott, *Range Imaging Laser Radar*, U. S. Patent 4,935,616, June 19, 1990.

2. J. Sackos, B. Bradley, B. Nellums, and C. Digert, "The Emerging Versatility of a Scannerless Range Imager," Laser Radar Technology and Applications Conference, SPIE AeroSense Symposium (Orlando, FL), paper #2748-4, (April 1996).

3. Capt. M. Keltos, "Demonstration of Imaging LADAR for Battle Damage Indication", 1998 Meeting of the IRIS Specialty Group on Active Systems, Albuquerque, NM, March 1998.

4. C. Digert, J. Sackos, and R. Nellums, "Building Accurate Geometric Models from Abundant Range Imaging Information," Laser Radar Technology and Application Conference, SPIE Aero Sense Symposium, Orlando, FL, April 1997.